



AFRL-RZ-WP-TP-2010-2249

NUMERICAL SIMULATION OF ETHYLENE INJECTION FROM IN-STREAM FUELING PYLONS (POSTPRINT)

Jason C. Doster, Paul I. King, and Raymond C. Maple

Air Force Institute of Technology

Mark R. Gruber

**Propulsion Sciences Branch
Aerospace Propulsion Division**

APRIL 2008

Approved for public release; distribution unlimited.

See additional restrictions described on inside pages

STINFO COPY

**AIR FORCE RESEARCH LABORATORY
PROPULSION DIRECTORATE
WRIGHT-PATTERSON AIR FORCE BASE, OH 45433-7251
AIR FORCE MATERIEL COMMAND
UNITED STATES AIR FORCE**

REPORT DOCUMENTATION PAGE

*Form Approved
OMB No. 0704-0188*

The public reporting burden for this collection of information is estimated to average 1 hour per response, including the time for reviewing instructions, searching existing data sources, gathering and maintaining the data needed, and completing and reviewing the collection of information. Send comments regarding this burden estimate or any other aspect of this collection of information, including suggestions for reducing this burden, to Department of Defense, Washington Headquarters Services, Directorate for Information Operations and Reports (0704-0188), 1215 Jefferson Davis Highway, Suite 1204, Arlington, VA 22202-4302. Respondents should be aware that notwithstanding any other provision of law, no person shall be subject to any penalty for failing to comply with a collection of information if it does not display a currently valid OMB control number. **PLEASE DO NOT RETURN YOUR FORM TO THE ABOVE ADDRESS.**

1. REPORT DATE (DD-MM-YY) April 2008			2. REPORT TYPE Conference Paper Postprint		3. DATES COVERED (From - To) 01 August 2007 – 28 April 2008	
4. TITLE AND SUBTITLE NUMERICAL SIMULATION OF ETHYLENE INJECTION FROM IN-STREAM FUELING PYLONS (POSTPRINT)					5a. CONTRACT NUMBER In-house	
					5b. GRANT NUMBER	
					5c. PROGRAM ELEMENT NUMBER 62203F	
6. AUTHOR(S) Jason C. Doster, Paul I. King, and Raymond C. Maple (Air Force Institute of Technology) Mark R. Gruber (AFRL/RZAS)					5d. PROJECT NUMBER 3012	
					5e. TASK NUMBER AI	
					5f. WORK UNIT NUMBER 3012AI00	
7. PERFORMING ORGANIZATION NAME(S) AND ADDRESS(ES) Air Force Institute of Technology (AFIT/ENY) 2950 Hobson Way Wright-Patterson AFB, OH 45433-7765			Propulsion Sciences Branch (AFRL/RZAS) Aerospace Propulsion Division Air Force Research Laboratory, Propulsion Directorate Wright-Patterson Air Force Base, OH 45433-7251 Air Force Materiel Command, United States Air Force		8. PERFORMING ORGANIZATION REPORT NUMBER AFRL-RZ-WP-TP-2010-2249	
9. SPONSORING/MONITORING AGENCY NAME(S) AND ADDRESS(ES) Air Force Research Laboratory Propulsion Directorate Wright-Patterson Air Force Base, OH 45433-7251 Air Force Materiel Command United States Air Force					10. SPONSORING/MONITORING AGENCY ACRONYM(S) AFRL/RZAS	
					11. SPONSORING/MONITORING AGENCY REPORT NUMBER(S) AFRL-RZ-WP-TP-2010-2249	
12. DISTRIBUTION/AVAILABILITY STATEMENT Approved for public release; distribution unlimited.						
13. SUPPLEMENTARY NOTES Conference paper published in the <i>Proceedings of the 15th AIAA International Space Planes and Hypersonic Systems and Technologies Conference</i> , conference held 28 April - 1 May 2008, in Dayton, OH. PA Case Number: AFIT PA 080367; Clearance Date: 28 Mar 2008. This is a work of the U.S. Government and is not subject to copyright protection in the United States						
14. ABSTRACT This paper covers numerical simulation results for an in-stream fuel injector in a Mach number 2.0 flow. Three fuel injection pylon configurations studied are a basic pylon, a ramp pylon, and an alternating wedge pylon. The first pylon configuration is a baseline. The latter two configurations introduce streamwise vorticity into the flow to increase mixing action. Computational Fluid Dynamic simulations with ethylene fuel injection are presented and evaluated. Four parameters used for comparison among the pylons are streamwise vorticity, total pressure loss, mixing efficiency, and flammable plume extent. An overall energy comparison is also accomplished. It is found the two pylons with streamwise vorticity generation are better mixing devices that have an energy advantage over the baseline for a finite distance downstream of the pylon.						
15. SUBJECT TERMS supersonic combustion, strut fuel injection, CFD						
16. SECURITY CLASSIFICATION OF: a. REPORT Unclassified			17. LIMITATION OF ABSTRACT: SAR	18. NUMBER OF PAGES 24	19a. NAME OF RESPONSIBLE PERSON (Monitor) Mark R. Gruber	
					19b. TELEPHONE NUMBER (Include Area Code) N/A	

Numerical Simulation of Ethylene Injection from In-stream Fueling Pylons

Jason C. Doster* and Paul I. King†

Air Force Institute of Technology, Wright-Patterson Air Force Base, OH 45433

Mark R. Gruber‡

Air Force Research Laboratory(AFRL/RZAS), Wright-Patterson Air Force Base, OH 45433

and

Raymond C. Maple§

Air Force Institute of Technology, Wright-Patterson Air Force Base, OH 45433

This paper covers numerical simulation results for an in-stream fuel injector in a Mach number 2.0 flow. Three fuel injection pylon configurations studied are a basic pylon, a ramp pylon, and an alternating wedge pylon. The first pylon configuration is a baseline. The latter two configurations introduce streamwise vorticity into the flow to increase mixing action. Computational Fluid Dynamic simulations with ethylene fuel injection are presented and evaluated. Four parameters used for comparison among the pylons are streamwise vorticity, total pressure loss, mixing efficiency, and flammable plume extent. An overall energy comparison is also accomplished. It is found the two pylons with streamwise vorticity generation are better mixing devices than have an energy advantage over the baseline for a finite distance downstream of the pylon.

I. Introduction

Intrusive fueling techniques for scramjet combustors are advantageous in distributing fuel uniformly over a combustor cross-section. The performance of a class of intrusive in-stream pylon injectors reported previously¹ is the focus of this paper. The current work provides numerical simulations of ethylene fuel injection from three geometric variants of the injector concept into a cold airflow at a Mach number of 2.0. The three pylon variants are designed to introduce varying degrees of streamwise vorticity into the flow to increase fuel/air mixing. The pylons are compared to determine which geometry results in the best fuel spreading and mixing into the main airflow. Total pressure losses are also of concern, so the spreading and mixing capabilities of each pylon are considered relative to the pressure loss they create.

II. Pylon Configurations

The three pylon configurations are: the basic pylon (Fig. 1), the ramp pylon (Fig. 2), and the alternating wedge pylon (Fig. 3). The construction of each pylon incorporates a two-piece forward and aft area. The forward area contains a plenum common to all pylon configurations. The aft area contains a constant angled compression ramp on the basic pylon and a hypermixer geometry on the other two pylons. The mating of the two pieces results in tall/thin rectangular injection slots created by the difference in the inner width of

*PhD Candidate, Dept of Aeronautics & Astronautics, Member AIAA

†Professor, Dept of Aeronautics & Astronautics, Senior Member AIAA

‡Senior Aerospace Engineer, AIAA Associate Fellow

§Assistant Professor, Dept of Aeronautics & Astronautics, Senior Member AIAA

the forward piece and the outer width of the aft piece. The common parameters for all pylons are: Height = 75 mm, Length = 103 mm, Frontal Blockage Area = 1215 mm², Fuel Port (Slot) Area = 57 mm², Front Wedge Angle = 14.7°, and Front Wedge Nose Radius = 1 mm.

The basic pylon configuration embodies the two fundamental fuel injection strategies of 1) maximizing fuel-air interface area by using a rectangular slot injector spanning a large percentage of the pylon height, and 2) injecting fuel upstream of the pylon aft area so fuel and air begin mixing prior to leaving the pylon surface. Figure 1 shows the basic pylon on a pedestal. The aft area of the basic pylon is a compression ramp at 10.6° (half angle) to the main airflow. The fueling slots operate at sonic conditions. A plenum in the forward area of the pylon provides fuel to the slots. This plenum is fed by an opening at the bottom of the pylon connected to the pedestal. Fuel injection is accomplished from a backward facing step that protects the injectant from the main flow for a short distance prior to joining the main airflow around the pylon.

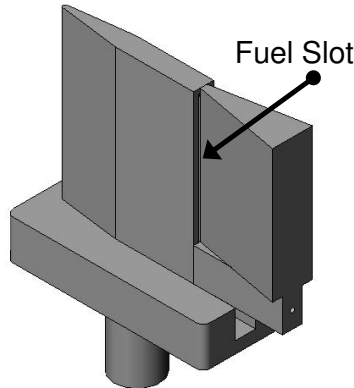


Figure 1. Basic pylon configuration.

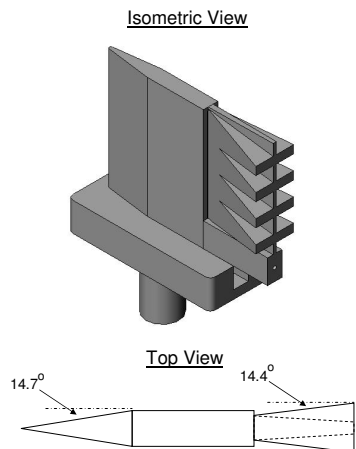


Figure 2. Ramp pylon configuration.

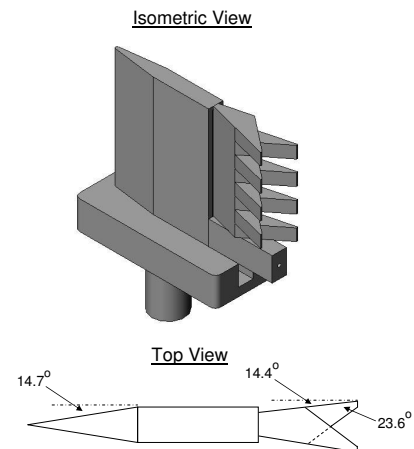


Figure 3. Alternating wedge pylon configuration.

The ramp pylon shown in Fig. 2 includes eight compression ramps on the aft area of the pylon. These compression ramps are 14.4° to the main airflow with 8.3° of ramp taper (sweep). Past studies have shown that sweep on a hypermixer compression ramp increases streamwise vortices and fuel/air mixing compared with no sweep.²⁻⁴ The compression and sweep angles were chosen to produce the same frontal blockage area as the basic pylon configuration.

The alternating wedge configuration shown in Fig. 3 includes eight alternating wedges on the aft area of the pylon. Past studies have indicated alternating wedge geometries also produce streamwise vortices and increase fuel/air mixing.^{5,6} The wedge geometries have a 23.6° angle and attach to the aft area of the pylon, itself having a 14.4° compression angle to the main airflow. This configuration is sized to produce the same frontal blockage area as the other two pylons.

III. Grid Construction

Grid generation is accomplished using a combination of GRIDGEN and SOLIDMESH. Boundary domains are constructed in GRIDGEN using imported surface geometry from the computer aided solid body design software SOLIDWORKS. These meshed surface domains are imported from GRIDGEN into SOLIDMESH and cells are constructed. The three dimensional grids for each pylon are an unstructured hybrid of rectangular/triangular surface domains and tetrahedral/pentahedral cell volumes. The viscous tailoring of the grid near the pylon boundary surfaces is accomplished to the refinement required to utilize the boundary layer wall functions in FLUENT ($30 < y+ < 200$). The initial wall spacing and grid refinement near the pylon boundary surfaces is the same for all three pylons. The exterior walls of the computational domain are inviscid for all three pylons in order to limit grid size, hence the grid is not refined near the outer walls. The wake region of all three pylons is populated with a dense cell mesh extending 290 mm downstream of the pylons. The cell volumes in the wake region are approximately 1 mm^3 . The grids for the three pylons vary between 5.5 - 6.7 million cells. Figure 4 shows a typical grid.

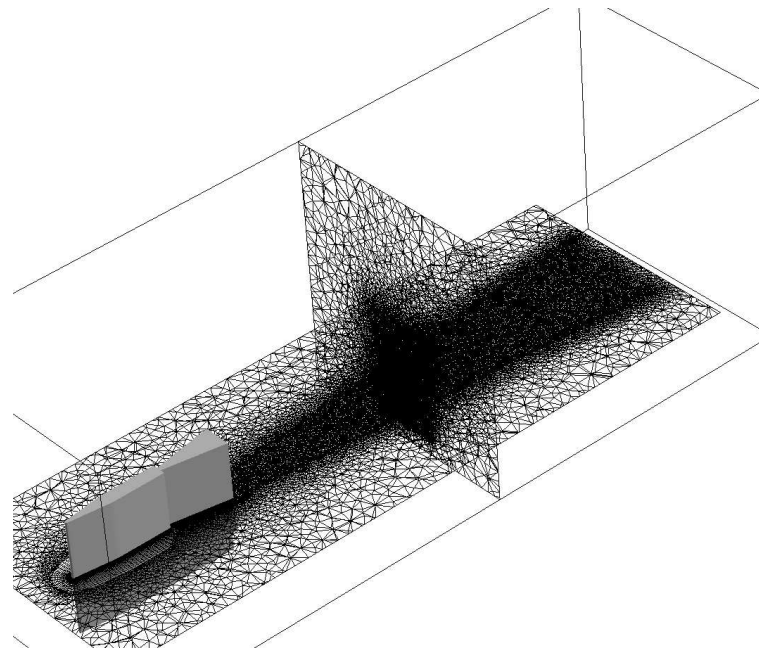


Figure 4. CFD internal grid.

Only one grid is constructed for each pylon. The grids are constructed similarly, with the most attention and refinement given to the wake region of the pylons. A grid convergence study is not accomplished to optimize the grids. Any comparison of these results to experimental data needs to take into account the inviscid exterior wall of these grid domains. Wind tunnel walls exhibit viscous effects. CFD solutions will be shown similar to experimental data at one plane location downstream of the pylons in a subsequent section.

IV. Flow Solution

FLUENT is the Computational Fluid Dynamics (CFD) code employed. The K- ω turbulence model with SST (shear stress transport) is used with a multi-species formulation of the compressible/viscous Navier Stokes flow equations. The result sought is a second order steady state or time accurate solution. No combustion is modeled, only species transport. The cold airflow inlet and ethylene injection conditions are shown in Table 1. These conditions result in a unity momentum flux ratio, q (Eq. 1).

$$q \equiv \frac{(\gamma PM^2)_{\text{ethylene}}}{(\gamma PM^2)_{\text{air}}} = \frac{(\rho u^2)_{\text{ethylene}}}{(\rho u^2)_{\text{air}}} \quad (1)$$

Table 1. Flow conditions for CFD simulation.

Property/Condition	Cold Airflow Inlet	Ethylene Injection
Ratio of Specific Heats	1.4	1.25
Molecular Weight	28.97	28.05
Mach Number	2.0	1.0
Velocity	518 m/s	314 m/s
Mass Flow	10.78 kg/s	0.04 kg/s
Total Temperature	300 K	300 K
Static Temperature	167 K	267 K
Total Pressure	310 KPa	320 KPa
Static Pressure	39.7 KPa	178 KPa
Flow Area	25,161 mm ²	57 mm ²

Solution convergence is determined three ways for a steady state solution: 1) the drag on the pylon is stable, 2) the residuals of mass, velocity, and energy are reduced at least three orders of magnitude from the original values, and 3) the spatially integrated total mass flow and ethylene mass flow are constant downstream of the pylons. Two of the three pylon solutions are steady enough to meet all three criteria given enough iterations of localized time-stepping. The third pylon exhibits a highly unsteady flow, and does not meet the mass flow requirement using localized time-stepping. Global time-stepping is implemented to find a time accurate flow solution for the third pylon.

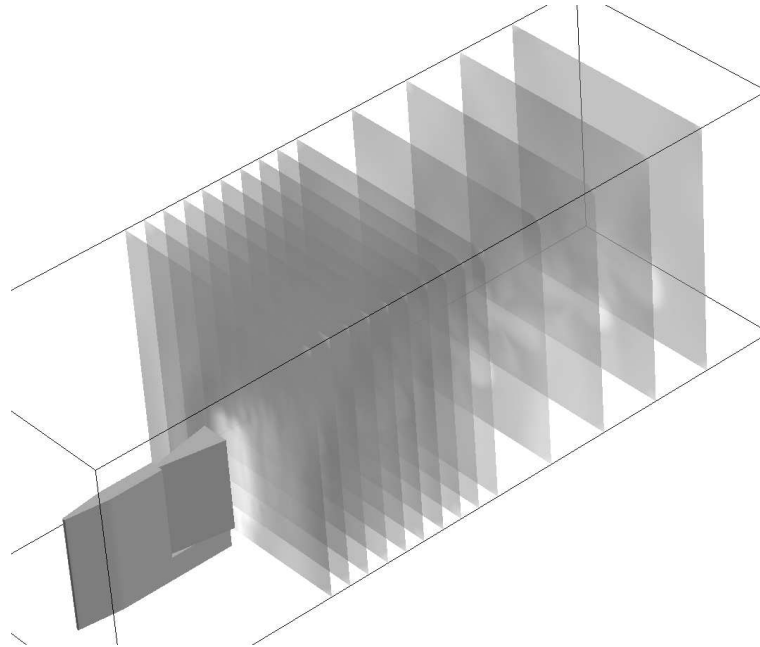


Figure 5. Data reduction planes.

V. Data Collection

The equivalent diameter, d_e , is the diameter of the rectangular slot fuel port area if it were to form a circle. The equivalent diameter for the fuel port area (57 mm^2) is 8.52 mm . The axial distance downstream of the injection slots is normalized by d_e . The dense cell wake region extends $34 d_e$ downstream of the pylon base (aft face), and the base of each pylon is 40 mm ($4.7 d_e$) aft of the injection slots.

Fourteen downstream positions are selected for reduction of five data parameters: streamwise vorticity, total pressure loss, mixing effectiveness, flammable plume extent, and potential work change ratio. These eight positions correspond to $5.9 d_e$, $7.4 d_e$, $8.9 d_e$, $10.6 d_e$, $12.1 d_e$, $13.6 d_e$, $15.3 d_e$, $16.8 d_e$, $18.3 d_e$, $20 d_e$, $24.7 d_e$, $29.4 d_e$, $34 d_e$, and $38.7 d_e$ aft of the injection slots. Figure 5 shows the fourteen downstream positions chosen for data reduction.

Streamwise vorticity, ω_x , is defined as the axial, or x-component, of the curl of the velocity vector. The absolute value of the quantity is used for the integration. The mass averaged integral of the absolute value of axial vorticity is the measure of streamwise vorticity, Ω_x (Eq. 2). Instead of presenting absolute numbers of streamwise vorticity, relative magnitudes are computed, normalized by the maximum vorticity value present in the data.

$$\begin{aligned} |\omega_x| &= \left| (\nabla \times \vec{V})_x \right| \\ \Omega_x &= \frac{\int |\omega_x| \rho u dA}{\int \rho u dA} \end{aligned} \quad (2)$$

Total pressure loss, Λ , is calculated from the mass averaged integral of total pressure. The mass averaged integral, divided by the wind tunnel total pressure and subtracted from unity, is the pressure loss (Eq. 3). Total pressure losses in this specific problem are relatively small (all three pylons block only 4.8% of the axial flow path area).

$$\begin{aligned} \bar{P}_T &= \frac{\int P_T \rho u dA}{\int \rho u dA} \\ \Lambda &= 1 - \frac{\bar{P}_T}{P_{T_{\text{tunnel}}}} \end{aligned} \quad (3)$$

Mixing effectiveness is quantified from a comparison of the local mass fraction of fuel/air to that for stoichiometric combustion. This method requires the injected fuel have a known stoichiometric fuel/air ratio, f_s . The mass fraction of fuel in air, α , can be calculated from f_s and the equivalence ratio, ϕ , with Eq. 4. For example, with $f_s = 0.068$, the mass fraction of ethylene in air at stoichiometric conditions ($\phi = 1$) calculated from Eq. 4 is $\alpha_s = 0.064$.

$$\begin{aligned} \alpha &= \frac{\text{mass of fuel}}{\text{mass of fuel} + \text{air}} \\ \alpha &= \frac{\phi f_s}{\phi f_s + 1} \end{aligned} \quad (4)$$

The mixing effectiveness formulation assumes the least available reactant, fuel or air, is the reactant considered for mixing. The other reactant is considered completely mixed already. For instance, in a globally fuel-lean situation (which is the case here), the fuel is the mixing concern, so the air is considered completely mixed. Equation 5 shows the mixing effectiveness quantity, η_m , in a globally fuel lean situation.^{7,8}

$$\begin{aligned} \eta_m &= \frac{\dot{m}_{\text{fuel,mixed}}}{\dot{m}_{\text{fuel,total}}} = \frac{\int_{A_{\alpha=0}} \alpha_R \rho u dA}{\int_{A_{\alpha=0}} \alpha \rho u dA} \\ \alpha_R &= \begin{cases} \alpha, & \alpha \leq \alpha_s \\ \alpha_s(1-\alpha)/(1-\alpha_s), & \alpha > \alpha_s \end{cases} \end{aligned} \quad (5)$$

The area of integration extends to the edges of the fuel plume where the fuel mass fraction drops to zero, or practically, to some minimum detection mass fraction, $\alpha \geq \alpha_{\min}$ ($\alpha_{\min} = 0.001$). If the local fuel mass fraction is less than the mass fraction required for stoichiometric combustion, the fuel is fully mixed. If the local fuel mass fraction is greater than the stoichiometric mass fraction, the fuel is unmixed to some degree. A weighting function, seen in the bottom line of Eq. 5, is used to quantify how unmixed is the local mass fraction. The fully mixed numerical value is one, and the completely unmixed numerical value is zero. This mixing effectiveness does not complete the fuel mixing picture. Mass fractions below stoichiometric, considered perfectly mixed, include those below the threshold for combustion. In addition, flammable mixtures exist above stoichiometric, and the formulation also does not take this into account. For a more complete picture, one must look at the flammable plume extent.

The flammable plume extent is observed in two quantities. First is the fuel plume area with mass fractions falling within the flammable region. This quantity is normalized by the injection slot area. Second is the fraction of fuel plume falling within the flammable region. The first quantity compares the overall flammable plume extent between pylons. The second quantity determines the most efficient place to ignite the flammable mixture, at the point where the fuel plume exhibits the largest fraction of flammable area. The equivalence ratio flammability limits for ethylene are used ($0.41 \leq \phi \leq 5.5$).⁹ Consequently, from Eq. 4, the range of flammable mass fractions of ethylene fuel in air is $0.027 \leq \alpha \leq 0.272$. The flammable plume area, FP_a , and the flammable plume fraction, FP_f , are shown in Eq. 6. The fuel injector area, A_e , is $5.7E-5 m^2$, and the fuel plume area, A_p , is the area of fuel having mass fractions greater than 0.001.

$$\begin{aligned} FP_a &= \frac{A_f}{A_e} \\ FP_f &= \frac{A_f}{A_p} \end{aligned} \quad (6)$$

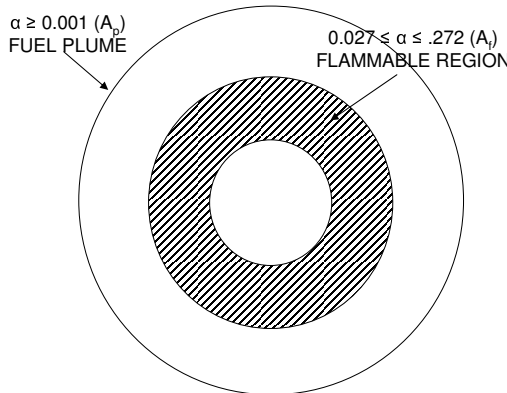


Figure 6. Fuel plume visual.

A measure is required to assess the overall performance of the pylons. There is energy loss due to reduction in flow total pressure. There is energy gain from heat release due to fuel mixing. The combination of this loss and gain is an energy change we shall call the work potential change of the combustor flow. Energy loss in a scramjet combustor normally includes drag losses (pressure and viscous) and heat release losses. During heat release in a scramjet combustor, total pressure and hence Mach number are reduced, decreasing the work potential of the combustor flow. Drag losses also appear as a total pressure loss, lowering the Mach number and the work potential of the combustor flow. Total pressure losses are entropy gains, as derived from the Gibbs equation and first law of thermodynamics (Eq. 7). Entropy gain results in a reduction in energy and work potential of the combustor flow.

$$\begin{aligned}
dq &= dh - vdP \\
\int ds &= C_p \int \frac{dT}{T} - R \int \frac{dP}{P} \\
\Delta s &= C_p \ln \frac{T_2}{T_1} - R \ln \frac{P_2}{P_1} = R \ln \left[\left(\frac{P_1}{P_2} \right) \left(\frac{T_2}{T_1} \right)^{\frac{1}{\gamma-1}} \right] \\
\Delta s &= R \ln \left(\frac{P_{t_1}}{P_{t_2}} \right) \\
\Delta W_L &= -\dot{m} T_1 \Delta s = -\dot{m} T_1 R \ln \left(\frac{P_{t_1}}{P_{t_2}} \right)
\end{aligned} \tag{7}$$

Energy gain from heat release in the combustor can be expressed through the first law of thermodynamics in Eq. 8. Heat addition is an augmentation in work potential of the combustor flow. The mixing efficiency parameter multiplied by the flammable plume fraction, $\eta_m FP_f$, is substituted for the combustion efficiency that should be present in the equation. Although not the combustion efficiency, this multiplied quantity allows for some calculation of the heat release. \dot{m}_f is the mass flow of fuel. h_f is heat release per kilogram of fuel. This equation offers some measure of the energy increase from fuel supplied by the pylon given the data available.

$$\Delta W_Q = \Delta Q = \dot{m}_f \eta_m FP_f h_f \tag{8}$$

The summation of energy gain due to heat addition and the energy loss due to entropy is a measure of the work potential change of the combustor flow due to pylon fueling (Eq. 9). This method omits effects due to heat release such as basic flow field changes, large pressure drops, and vorticity/mixing rate changes. However, in the absence of a defined combustor geometry, we believe this approach is a reasonable alternative to a full examination of a scramjet flow path incorporating these pylons.

$$\Delta W = \Delta W_L + \Delta W_Q = \dot{m}_f \eta_m FP_f h_f - \dot{m} T_1 R \ln \left(\frac{P_{t_1}}{P_{t_2}} \right) \tag{9}$$

The work potential change is a representative quantity, meant only to compare the performance of each pylon, not to predict the actual work potential in a combustor. In presentation, the work potential change of the alternating wedge and ramp pylons are divided by the work potential change of the basic pylon to give a work potential change ratio.

VI. Numerical Simulation Results

The basic pylon exhibits highly unsteady flow in the form of vortex shedding. Localized time stepping results in reduced residuals about three orders of magnitude from original values, and a steady drag on the pylon, but the total mass flow downstream of the pylon is not constant. The total mass flow decreases and the ethylene mass flow increases in magnitude in the downstream direction. This is a violation of mass conservation. A time accurate solution is needed for this pylon. An estimate of the vortex shedding frequency is accomplished to calculate a time step required to resolve the unsteadiness in the wake flow. A Strouhal number of 0.25 is assumed as a typical non-dimensional shedding frequency downstream of bluff bodies in high Reynolds number flows. The flow velocity is 518 m/s and the width of the pylon base is 0.018 m. Given Eq. 10, the vortex shedding frequency estimated is about 7200 Hz.

$$St = \frac{fd}{V} \tag{10}$$

A time step of one microsecond is selected to resolve this shedding frequency. Monitoring the Mach number of three points in the wake region of the pylon, the flow solution is advanced in time until a

consistent periodic pattern emerges. Figure 7 shows the Mach number over time at one of the three points. The same periodic frequency is observed at all three points, approximately 6900 Hz ($St = 0.24$).

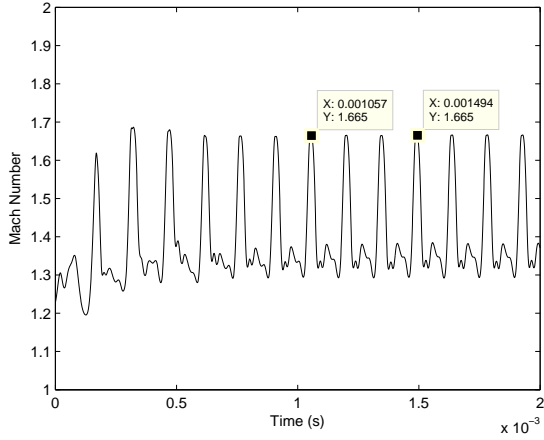
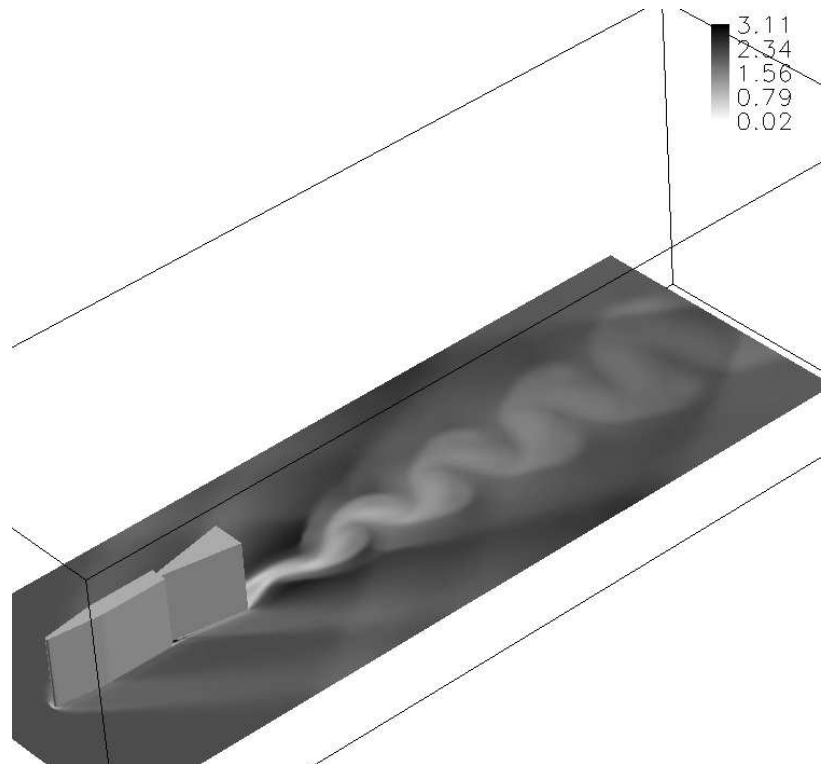


Figure 7. Mach number at point in wake region over time.

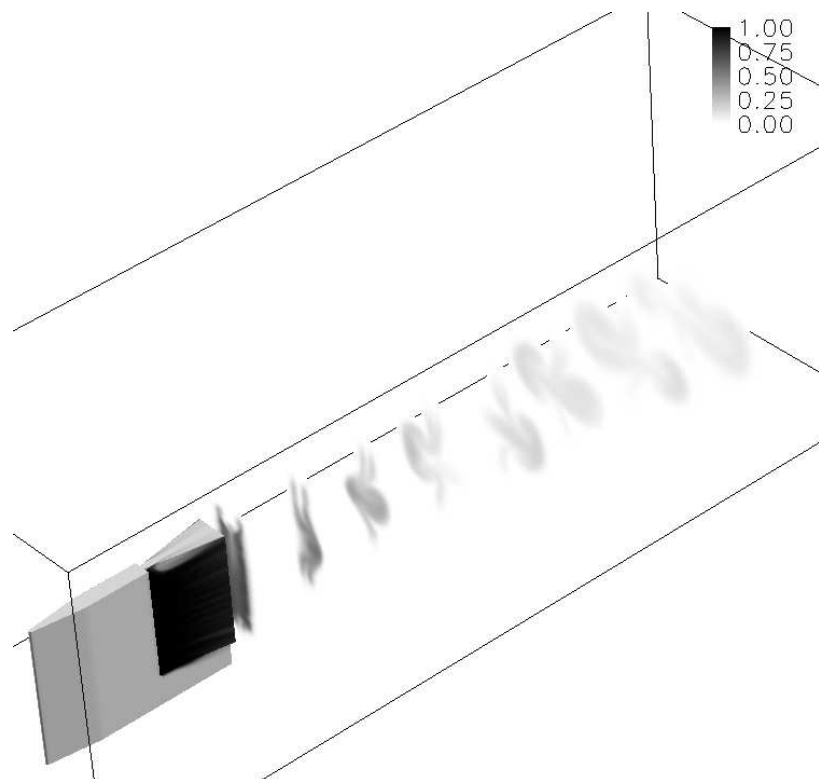
The solution at the final time step is kept for analysis. The solution is then advanced one half period further, and that solution is also kept for analysis. Data collection is accomplished at the eight downstream planes in both instantaneous snapshots, one half period separated, and averaged. As it turns out, all the integrated quantities are virtually identical in the two time snapshots.

A planar cut in the y-direction of the Mach number half way up the basic pylon height and eight planar cuts in the x-direction of ethylene mass fraction downstream of the pylon are shown in Fig. 8. Only the first of the time solution points is displayed. The other time point is very similar, where the vortex shedding is at a different point in its phase.

The ramp and alternating wedge pylons both exhibit a constant mass flow in their wake region and meet the other steady state solution convergence criteria using localized time stepping. This is not to say the flow downstream of these pylons is perfectly steady, just steady enough to satisfy the convergence criteria selected. It appears the streamwise vorticity production of the ramp and alternating wedge pylons promotes a more steady flow in the wake region. Vortex shedding is not present in these solutions. The same planar cuts of Mach number and ethylene mass fraction are displayed for the ramp and alternating wedge pylons in Figs. 9 and 10.

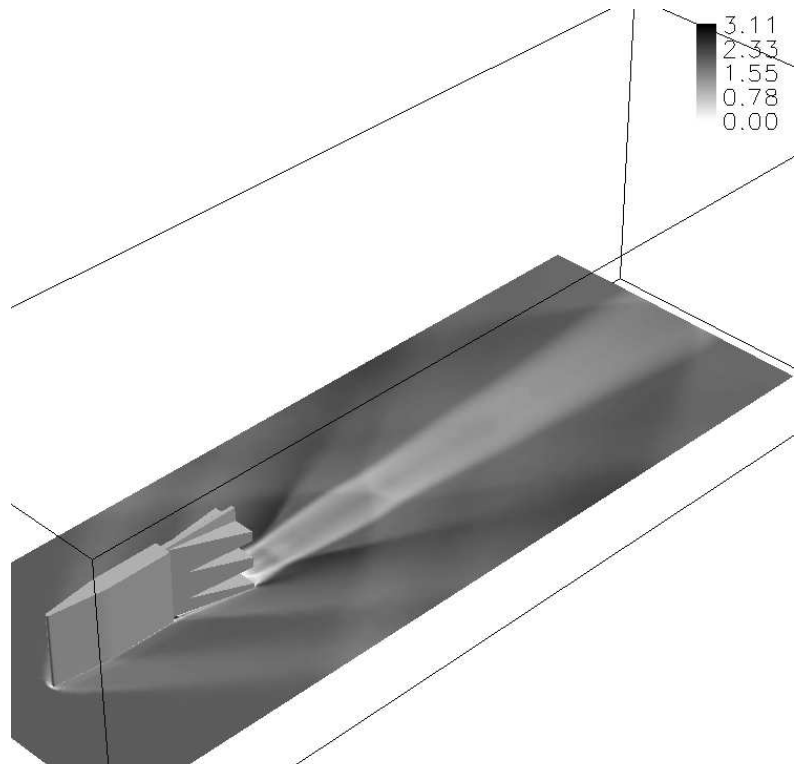


(a) Mach number.

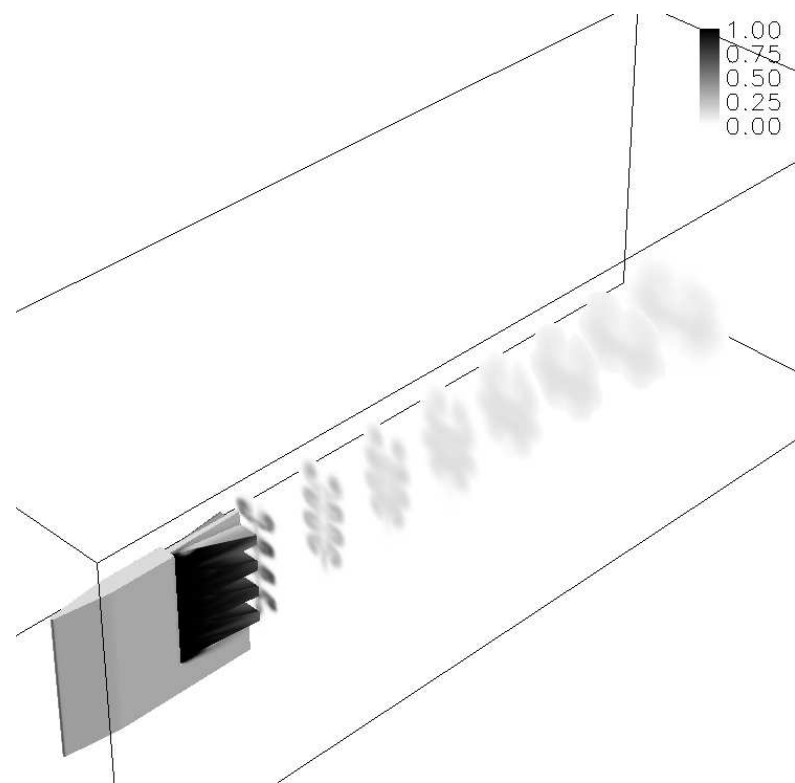


(b) Ethylene mass fraction.

Figure 8. Basic pylon.

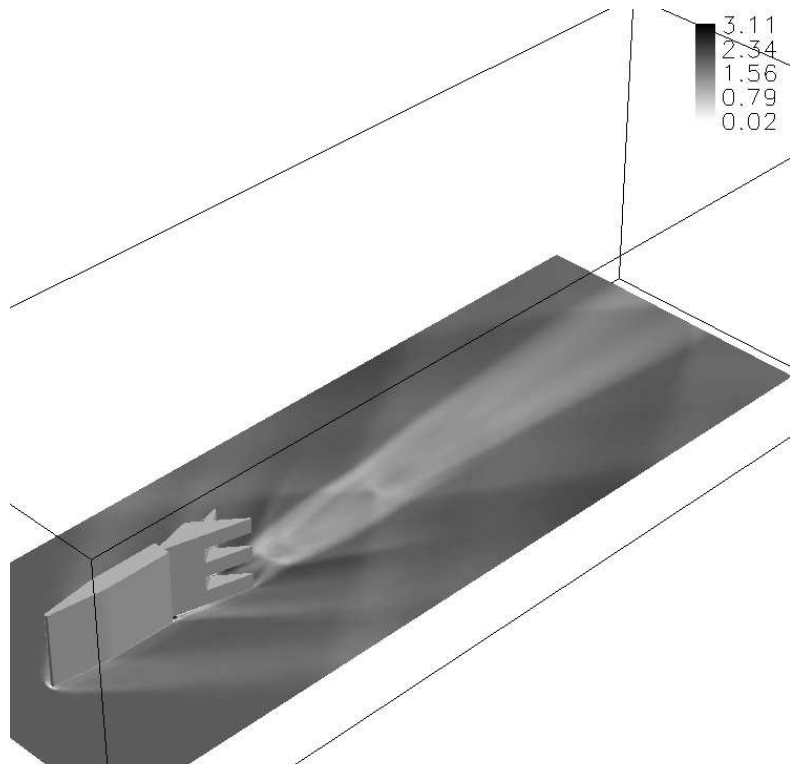


(a) Mach number.

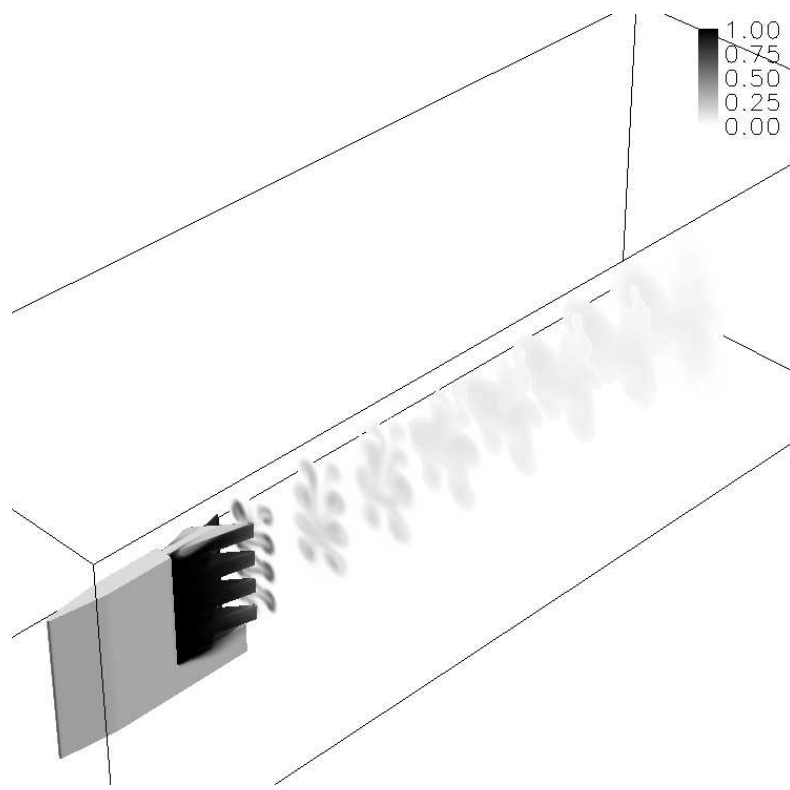


(b) Ethylene mass fraction.

Figure 9. Ramp pylon.



(a) Mach number.



(b) Ethylene mass fraction.

Figure 10. Alternating wedge pylon.

VII. Pylon Comparisons

In general, the most interesting comparison area between pylon wake flows is from the pylon base to approximately $20 d_e$. The mass flows in the wake region of the three pylons are compared in Fig. 11. For the two steady solutions, the total mass flow and ethylene mass flow are constant in the wake region. For the time accurate solution, the total mass flow and ethylene mass flow in the wake region vary slightly, but do not on average increase or decrease with downstream distance. The mass flows oscillate around the correct values of 10.82 kg/s and 0.04 kg/s respectively.

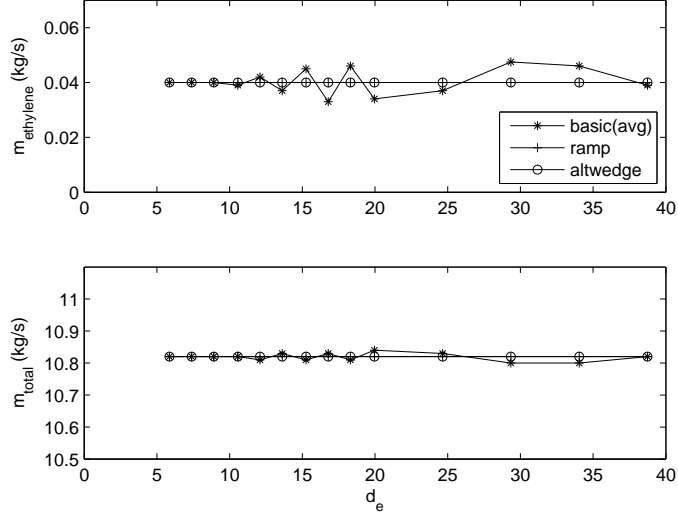


Figure 11. Mass flow comparison.

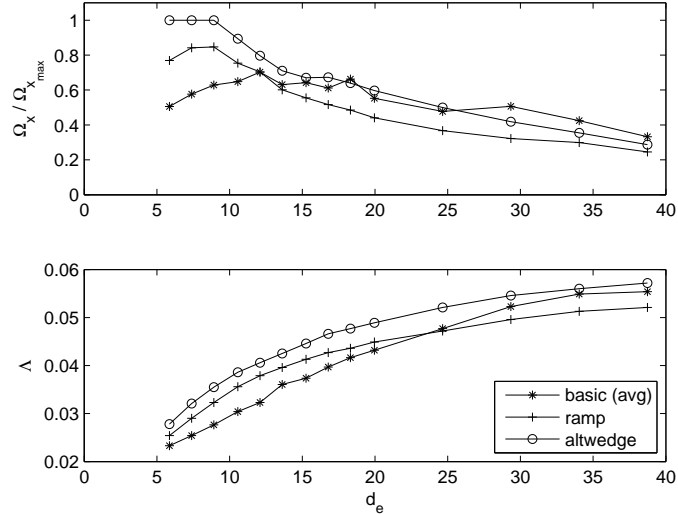


Figure 12. Vorticity and pressure loss comparison.

The streamwise vorticity and pressure loss produced by the three pylons are compared in Fig. 12. It is difficult to make direct downstream position comparisons between the basic pylon and the other two with the slight mass flow variations in the basic pylon time accurate solution. However there are general trends. The general trend for streamwise vorticity is to decrease with downstream distance. The general trend for pressure loss is to increase with downstream distance. The vorticity present immediately downstream of the

ramp and alternating wedge pylons is increased over the basic pylon due to the vortical inducing geometries at the aft end of those pylons. However, the increased vorticity of these geometries is observed for a short distance. In this narrow window of space is the opportunity for the ramp and alternating wedge pylons to mix fuel and air more rapidly than the basic pylon. Looking past the near-field, the streamwise vorticity downstream of the basic pylon exceeds that of ramp pylon and the alternating wedge pylon as downstream distance increases into the far-field. The pressure loss of the basic pylon exceeds that of the ramp pylon as downstream distance increases into the far-field, but does not exceed the pressure loss of the alternating wedge pylon.

Overall, the increased streamwise vorticity of the ramp and alternating wedge pylons in the near-field wake region comes with added pressure loss over the basic pylon. As downstream distance increases into the far-field, the basic pylon comes close to or exceeds the ramp and alternating wedge pylons in vorticity and pressure loss. The alternating wedge pylon has larger vorticity and pressure loss than the ramp throughout the wake region.

The non-dimensional drag from surface pressures is the drag coefficient, which is defined in Eq. 11. The dynamic pressure multiplied by the pylon frontal area is 134.9 N in this cold flow for all pylons since each has the same frontal area by design. The drag coefficients are presented in Table 2.

$$C_d = \frac{Drag}{\frac{1}{2}\rho u^2(Area)} = \frac{Drag}{\frac{\gamma}{2}PM^2(Area)} \quad (11)$$

Table 2. Pylon drag.

Pylon	C_d	Drag (Newtons)
Basic	0.61	82
Ramp	0.59	80
Alternating Wedge	0.66	89

The mixing efficiency of the pylons is shown in Fig. 13. In general mixing efficiency increases with downstream distance. The alternating wedge pylon exhibits the greatest mixing efficiency of all the pylons throughout the wake region. The ramp pylon shows a reduced mixing efficiency to the alternating wedge pylon, and exceeds the mixing efficiency of the basic pylon in most of the wake region. The basic pylon has a reduced mixing efficiency compared to both the alternating wedge and ramp pylons until the very end of the wake region computed.

The flammable plume extent is shown in Fig. 14. The alternating wedge pylon has the largest flammable plume area throughout the wake region. The ramp pylon has the second largest flammable plume area in most of the wake region, however, the basic pylon flammable plume area matches the ramp pylon as downstream distance increases. The flammable plume fractions reveal the most advantageous location to ignite the fuel plumes. The alternating wedge and ramp pylons both show a rise to maximum flammable plume fraction, $10 d_e$, upstream of the basic pylon rise to maximum flammable plume fraction, $20 d_e$. The ramp and alternating wedge pylons have larger fractions of the fuel plume ready for combustion in a shorter downstream distance than the basic pylon. Between the the ramp and alternating wedge pylons, the flammable plume fraction of the alternating wedge rises slightly faster in the near-field region.

A last comparison is to examine the tradeoff between pressure loss created by each pylon versus the potential heat energy they could produce through mixing the injected fuel. This comparison is made at each of the eight positions in the wake region. Equation 9, potential work change, is the method of comparison. At each axial position in the wake region the mass flow of ethylene (\dot{m}_f), the total mass flow (\dot{m}), the inverse total pressure loss ratio ($(1 - \Lambda)^{-1}$), the mixing efficiency (η_m), and the flammable plume fraction (FP_f) are calculated. These measures are used in the tradeoff calculation. The other variables in the equation are held constant. $h_f = 4.5E7 \text{ J/kg}$: this is a typical heating value for a hydrocarbon fuel. $R = 287 \text{ J/kg K}$: although ethylene has a different gas constant, it is in the minority, so the gas constant of air is used. $T_1 = 712 \text{ K}$: this is a typical combustor inlet static temperature, calculated in previous work.¹ The ratio of potential work change between the ramp and alternating wedge pylons compared to the basic pylon is shown in Fig. 15.

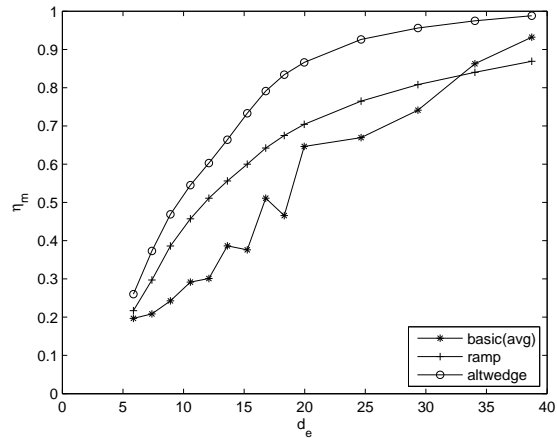


Figure 13. Ethylene/air mixing comparison.

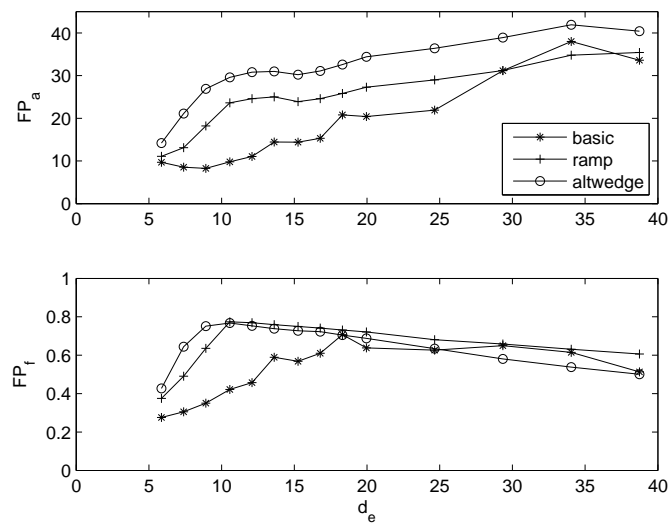


Figure 14. Flammable plume comparison.

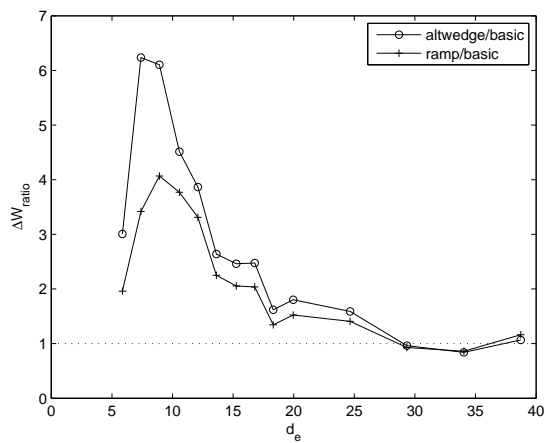


Figure 15. Potential work comparison.

The alternating wedge and ramp pylons both exceed the basic pylon in potential work change for a large portion of the wake region. It is noteworthy that the basic pylon matches the ramp and alternating wedge pylons around $29 d_e$. At this point the two hypermixer pylons loose their energy advantage over the basic pylon. However, the flammable plume mixture downstream of the hypermixer pylons is ready for combustion around $10 d_e$, and they still have the energy advantage over the basic pylon at that location. In summary, there is a finite distance downstream where the alternating wedge and ramp pylons perform better than the basic pylon. Between the two hypermixer pylons, the alternating wedge pylon out performs the ramp pylon slightly.

VIII. Comparison to Experiment

A qualitative comparison of simulation and initial experimental data obtained is presented. There are some differences in conditions between simulation and experiment. The inviscid walls of the simulation versus the viscous walls of the experiment is one difference. Also, the primary flow Mach number is 2.0 in the simulation and 1.95 in the wind tunnel experiment. The ramp and alternating wedge pylon simulations are compared to experiment since they have a reasonably steady wake flow. The data gathered in the wind tunnel was done using a static pressure cone probe and a total pressure pitot probe, yielding averages at a measurement point. The wind tunnel probing location is 6.44 inches downstream of the pylon ($23.9 d_e$), and the probing area is 2 in x 3 in extent. Figure 16 shows the probing area in relation to the pylon.

Mach number is the parameter chosen for comparison. The ramp and alternating wedge pylons both show similar wake region shapes and Mach number magnitudes in experiment and simulation (Fig. 17 and 18). The resolution of the simulation data is much better than experiment. The probing area holds approximately 3500 simulation cells, and only 225 probing locations. One notable difference in the Mach profiles is the side areas. The experimental results show higher Mach numbers on the sides. This is most likely due to the reflection of the shock wave off the wall being in a different location due to the wall boundary layer present in the wind tunnel experiment, but not in the simulation. The position of the reflected shock could also account for the slight differences in the shapes of the pylon wakes. Overall, the Mach profiles are similar in simulation and experiment for these two pylons.

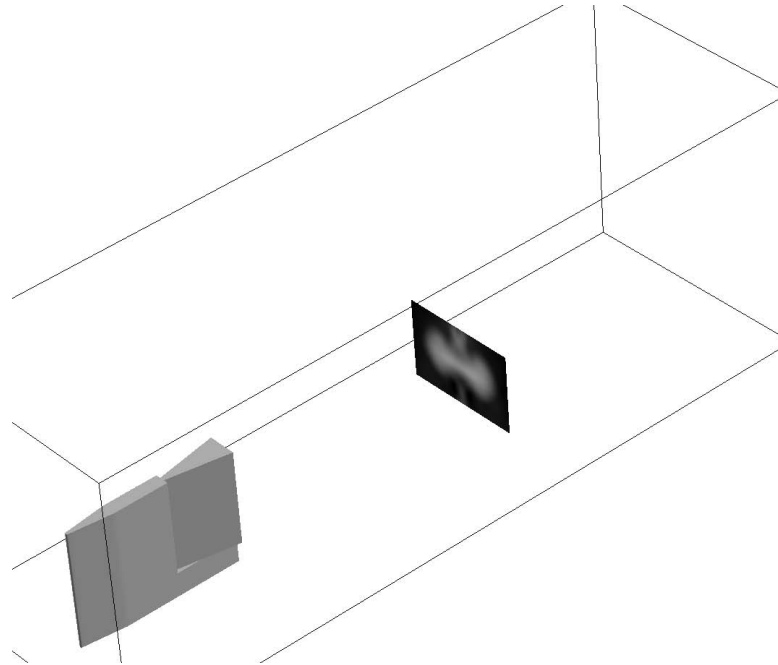


Figure 16. Wind tunnel probing area.

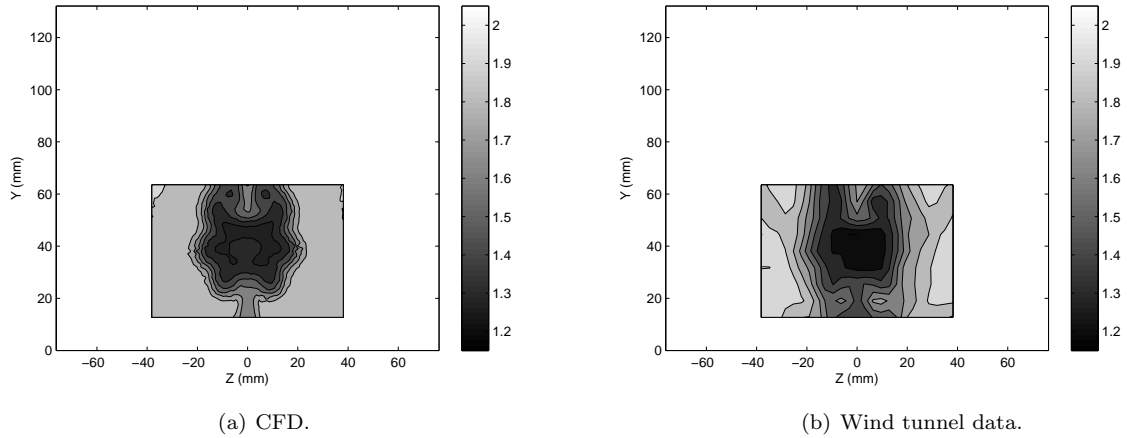


Figure 17. Ramp pylon Mach number.

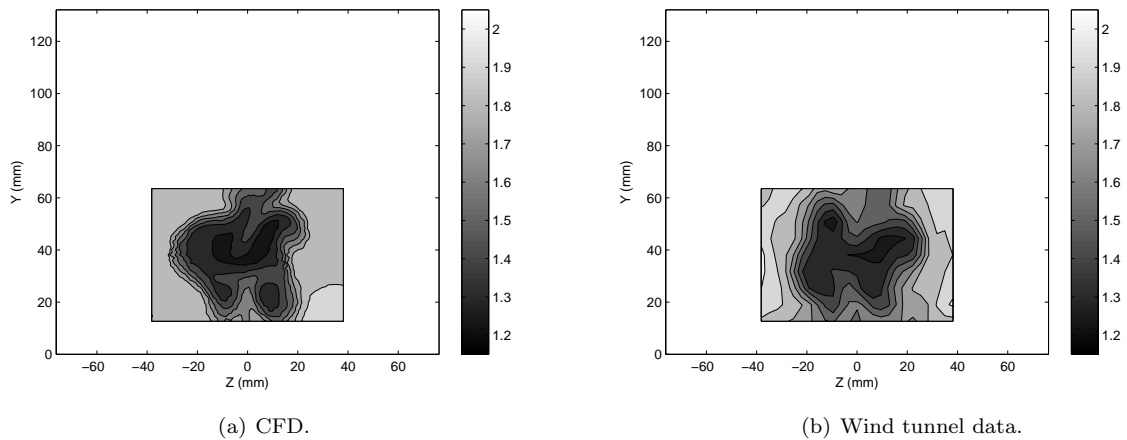


Figure 18. Alternating wedge pylon Mach number.

IX. Conclusions

Three pylons are compared in their performance as in-stream scramjet fuel injectors. All three pylons exhibit the same frontal area to the flow. A cold flow CFD study with ethylene fuel injection is accomplished for each pylon. The ramp and alternating wedge pylons show decisive near-field wake region increases in axial vorticity compared to the basic pylon. They also exhibit an increase in total pressure loss accompanying the increased streamwise vorticity. The increased vortical motion results in better mixing characteristics for those pylons, bringing the ethylene/air mixture to flammable conditions in a shorter distance. This promotes the idea that streamwise vorticity production can be used to shorten combustor lengths. A theoretical energy comparison also shows that the ramp and alternating wedge pylons have an energy advantage over the basic pylon for a finite distance downstream of the pylon if the fuel plume is ignited within this distance. A last observation is the alternating wedge pylon has a slight performance advantage over the ramp pylon.

The views expressed in this article are those of the authors and do not reflect the official policy or position of the United States Air Force, Department of Defense, or the U.S. Government.

References

¹Doster, J., King, P., Gruber, M., and Maple, R., "Pylon Fuel Injector Design for a Scramjet Combustor," AIAA Paper 2007-5404, 2007.
²Northam, G., Greenberg, I., and Byington, C., "Evaluation of Parallel Injector Configurations for Supersonic Combus-

tion," AIAA Paper 89-2525, Jul. 1989.

³Riggins, D., Mekkes, G., McClinton, C., and Drummond, J., "A Numerical Study of Mixing Enhancement in a Supersonic Combustor," AIAA Paper 90-0203, Jan. 1990.

⁴Abdel-Salam, T., Tiwari, S., Chaturvedi, S., and Mohieldin, T., "Mixing and Combustion in Scramjet Combustor with Raised and Relieved Ramp," AIAA Paper 2000-3709, Jul. 2000.

⁵Sunami, T. and Scheel, F., "Analysis of Mixing Enhancement Using Streamwise Vortices in a Supersonic Combustor by Application of Laser Diagnostics," AIAA Paper 2002-5203, Oct. 2002.

⁶Sunami, T., Magre, P., Bresson, A., Grisch, F., Orain, M., and Kodera, M., "Experimental Study of Strut Injectors in a Supersonic Combustor Using OH-PLIF," AIAA Paper 2005-3304, May 2005.

⁷Mao, M., Riggins, D., and McClinton, C., "Numerical Simulation of Transverse Fuel Injection," Tech. Rep. N91-21097, NASA Langley Research Center, Hampton, VA 23665.

⁸Fuller, R., Wu, P., Nejad, A., and Schetz, J., "Comparison of Physical and Aerodynamic Ramps as Fuel Injectors in Supersonic Flow," Journal of Propulsion and Power, Vol. 14, No. 2, Mar.-Apr. 1998, pp. 135-145.

⁹Glassman, I., Combustion, Academic Press, 1996.